







Article

InP/Si₃N₄ Hybrid Integrated Lasers for RF Local Oscillator Signal Generation in Satellite Payloads

Jessica César-Cuello ^{1,*} , Alberto Zarzuelo ¹, Robinson C. Guzmán ² , Charoula Mitsolidou ³, Ilka Visscher ³ , Roelof B. Timens ³ , Paulus W. L. Van Dijk ³, Chris G. H. Roeloffzen ³, Luis González ¹, José Manuel Delgado Mendinueta ¹  and Guillermo Carpintero ¹ 

- ¹ Electronics Department, Carlos III University of Madrid, 28911 Madrid, Spain; azarzuel@pa.uc3m.es (A.Z.); lgguerre@ing.uc3m.es (L.G.); jodelgad@ing.uc3m.es (J.M.D.M.); guiller@ing.uc3m.es (G.C.)
- ² Department of Communications and Signal Theory and Computer and Telematic Systems, Universidad Rey Juan Carlos, 28942 Madrid, Spain; robinson.guzman@urjc.es
- ³ Lionix International B.V, 7521 AN Enschede, The Netherlands; c.mitsolidou@lionix-int.com (C.M.); i.visscher@lionix-int.com (I.V.); r.b.timens@lionix-int.com (R.B.T.); p.w.l.vandijk@lionix-int.com (P.W.L.V.D.); c.g.h.roeloffzen@lionix-int.com (C.G.H.R.)
- * Correspondence: jecesarc@ing.uc3m.es

Abstract: This paper presents an integrated tunable hybrid multi-laser module designed to simultaneously generate multiple radiofrequency (RF) local oscillator (LO) signals through optical heterodyning. The device consists of five hybrid InP/Si₃N₄ integrated lasers, each incorporating an intracavity wavelength-selective optical filter formed by two micro-ring resonators. Through beating the wavelengths generated from three of these lasers, we demonstrate the simultaneous generation of two LO signals within bands crucial for satellite communications (SatCom): one in the Ka-band and the other in the V-band. The device provides an extensive wavelength tuning range across the entire C-band and exhibits exceptionally narrow optical linewidths, below 40 kHz in free-running mode. This results in ultra-wideband tunable RF signals with narrow electrical linewidths below 100 kHz. The system is compact and highly scalable, with the potential to generate up to 10 simultaneous LO signals, being a promising solution for advanced RF signal generation in high throughput satellite payloads.

Keywords: hybrid integrated laser; integrated microwave photonics; satellite communications



Received: 17 December 2024
Revised: 10 January 2025
Accepted: 13 January 2025
Published: 16 January 2025

Citation: César-Cuello, J.; Zarzuelo, A.; Guzmán, R.C.; Mitsolidou, C.; Visscher, I.; Timens, R.B.; Dijk, P.W.L.V.; Roeloffzen, C.G.H.; González, L.; Delgado Mendinueta, J.M.; et al. InP/Si₃N₄ Hybrid Integrated Lasers for RF Local Oscillator Signal Generation in Satellite Payloads. *Photonics* **2025**, *12*, 77. <https://doi.org/10.3390/photonics12010077>

Copyright: © 2025 by the authors. Licensee MDPI, Basel, Switzerland. This article is an open access article distributed under the terms and conditions of the Creative Commons Attribution (CC BY) license (<https://creativecommons.org/licenses/by/4.0/>).

1. Introduction

Microwave photonics is key technology for the development of flexible radiofrequency (RF) payloads. Photonics technology offers critical advantages, such as enhanced system re-configurability, reduced size, weight, and power consumption (SWaP), as well as increased bandwidth, all of which are essential for modern satellite applications [1–3]. Integrated microwave photonics (iMWP) further enhances these benefits by combining microwaves and photonic integration, enabling functions such as signal generation and processing directly on a photonic integrated circuit (PIC) to improve scalability, stability, and overall system cost efficiency, while offering even greater SWaP reductions [4]. Different photonic integration platforms supporting PIC design and fabrication have been developed, each offering standardized process design kits (PDKs). Among these platforms, it is worth highlighting thin-film lithium niobate (TFLN) [5,6], indium phosphide (InP) [7,8], and silicon nitride (Si₃N₄) [9,10], as well as hybrid solutions such as InP/Si₃N₄ [11,12], providing a range of options for tailored iMWP implementations.

In a photonic-based RF payload, the RF signal generation unit is a key module [1]. This unit is responsible for the generation and distribution of the local oscillator (LO) signal. To achieve RF signals over a broad frequency range, optical heterodyning is a commonly employed technique. This process involves mixing two optical wavelengths on a high-speed photodetector (HS-PD), which generates an RF beat signal at a frequency corresponding to the difference between the two wavelengths [13–17]. To date, the two main photonic integration platforms that have been used for optical heterodyne RF signal generation are monolithic InP and hybrid InP/Si₃N₄. An example of a monolithic implementation, detailed in [14], utilizes an InP-based photonic integrated circuit for terahertz (THz) signal generation. This chip integrates two distributed feedback (DFB) lasers to generate electrical signals within the THz range. An experimental setup for THz transmission was also developed, featuring a transmitter based on a waveguide-integrated PIN photodiode and a receiver employing an InGaAs/InAlAs-based photoconductor. On the other hand, RF signal generation was recently demonstrated using a hybrid InP/Si₃N₄ integrated circuit, highlighting the wide RF frequency tuning range, from 5 GHz to 155 GHz [17]. A key distinction between InP DFB lasers and hybrid InP/Si₃N₄ lasers is their optical linewidth in free-running conditions. The DFB lasers have optical linewidths in the tens-of-MHz range, requiring the use of a stabilization scheme to reduce their optical linewidth [18], thereby lowering the electrical linewidth of the generated RF signal. In contrast, the signals generated by the InP/Si₃N₄ dual-laser module presented in [17] showed an electrical linewidth of less than 150 kHz under free-running conditions, with a long-term drift of less than 12 MHz, without requiring phase-locking techniques. This improved performance is attributed to the low propagation losses (0.1 dB/cm) of the TriPleX[®] Si₃N₄ waveguides [19], which enable longer cavity lengths and high Q-factor resonators, resulting in narrower linewidths. Furthermore, lasers with intrinsic linewidths as narrow as 40 Hz have been successfully demonstrated on this platform [20].

In this paper, we report for the first time, to the best of our knowledge, the generation of dual local oscillator signals from a hybrid multi-laser module. This module serves as the core component of a photonic RF channel multiplexing/demultiplexing subsystem designed for flexible satellite payloads under the THORMUX (Tunable Photonic RF Demultiplexer for Broadband Satellites) project, funded by the European Space Agency (ESA). The primary objective of THORMUX is the development of a 4-channel photonic-based multiplexer/demultiplexer (MUX/DEMUX) system capable of performing efficient RF multiplexing and demultiplexing operations in the Ka-, Q-, and V-bands.

THORMUX operates using three PICs modules PIC_1: the carrier generation system, which is the module presented in this work; PIC_2: incorporates single side-band carrier re-injection (SSB-CRI) filters; and PIC_3: contains a 4-channel MUX/DEMUX filter. The operating principle of the overall system is as follows: an optical carrier at a wavelength of 1550 nm is generated by a laser integrated in the PIC_1 module. During demultiplexing, the optical carrier is split into five outputs via a 1-to-5 optical power splitter. One of the outputs is directed to an optical Mach–Zehnder modulator (MZM), which converts the incoming RF signal into an optical double side-band full carrier (DSB-FC) signal. This signal consists of the lower sideband (LSB), the carrier, and the upper sideband (USB). The RF input signal can operate within the Ka, Q, or V frequency bands. The optically modulated DSB-FC signal is then routed to the single sideband (SSB) filter within the module PIC_2, which suppresses the unwanted LSB and the carrier while allowing the USB to pass through without distortion. The resulting USB signal is subsequently demultiplexed into four distinct optical channels by the DEMUX filter within the PIC_3 module. Each demultiplexed USB channel is then combined with the re-injected carrier signals derived from the remaining four outputs of the 1 × 5 splitter. This operation is performed via the

respective SSB-CRI filters in PIC_2. Finally, the processed optical channel signals are sent to a photodiode (PD) array, where optical-to-electrical conversion is achieved through a beating process.

During multiplexing, the process is similar but operates in reverse. Each channel uses a dedicated laser from PIC_1 and an individual modulator. This bidirectional operation is facilitated by the module PIC_3. The four multiplexed optical channels are aggregated into a single output, directed to a unique output photodiode.

The project is motivated by the need to overcome the limitations of conventional RF systems. For example, analog RF systems typically operate at fixed frequencies, which inherently limits tuning flexibility. Furthermore, digital RF channelization systems, such as those offered by Teledyne Technologies, provide greater flexibility but are limited in terms of maximum operating frequency. In addition, the SWaP metrics of these systems are not optimal due to the high-power consumption (on the order of 30–100 W) associated with the field-programmable gate arrays (FPGAs) used in the signal digitization processes and the up- and down-converters.

While the primary focus of the project is on the Ka-, Q- and V-bands, the photonic approach adopted enables operation beyond these frequency ranges while maintaining full flexibility. A critical aspect of this methodology is the establishment of a technology roadmap aimed at improving the performance and scalability of next-generation communications systems, with a particular focus on satellite-based applications.

The paper is organized into the following sections. Section 2 provides a detailed description of the hybrid multi-laser module characterized in this study, along with an introduction to the hybrid lasers used for signal generation. Section 3 presents the experimental characterization of the lasers, focusing on the generation and frequency flexibility of the local oscillator signals produced by the module. Section 4 provides a detailed discussion of the results, analyzing the performance and highlighting the key findings related to the system's capabilities. Finally, Section 5 provides the conclusions drawn from this study.

2. Hybrid Multi-Laser Module

Figure 1 shows the hybrid multi-laser module, which consists of five integrated InP/Si₃N₄ hybrid lasers: a dual-gain laser (laser 1, intended for optical frequency comb generation) and four single-gain lasers (lasers 2 through 5, intended for optical heterodyning). The lasers are mounted on a common thermally stabilized base, with thermal stabilization provided by a Peltier, a temperature controller (TEC), and an NTC thermistor. The core of the hybrid multi-laser module consists of a 1.6 cm × 2.74 cm TriPleX[®] PIC from LioniX (Enschede, The Netherlands), six InP gain sections developed by Fraunhofer HHI (Berlin, Germany), and two fiber arrays, all mounted on a copper submount. The module has a final footprint of 74 mm × 122.2 mm and was operated at a constant temperature of 21 °C during all measurements. All relevant electronics are mounted on an “n”-shaped base plate.

Dual LO generation is demonstrated in this work, using three out of the four single-gain lasers. The layout of the four single-gain lasers is presented in Figure 2. The hybrid laser was created through butt coupling an InP quantum well (QW) gain chip and a passive Si₃N₄ chip (highlighted by a dashed red box). The Si₃N₄ PIC includes two coupled micro-ring resonator mirrors with slightly different Free Spectral Ranges (FSRs), 208 GHz for micro-ring resonator 1 (top) and 215 GHz for micro-ring resonator 2 (bottom). This configuration enables single-frequency operation through the Vernier effect [21], since the difference in FSRs allows only one wavelength to be aligned in both micro-resonators at a time, suppressing other modes. This selection scheme results in single-frequency operation because the overlapping resonant wavelengths create a unique feedback condition that

stabilizes the laser at a single, well-defined frequency. Thus, the Vernier effect enables selective resonance by tuning only a single frequency within the external cavity. As shown in Figure 2, the cavity includes five phase thermo-optic actuators (heaters): one (H1) to determine the frequency positions of the cavity modes, two (H2 and H3) to control the light levels entering and exiting the laser cavity, and two (R1 and R2) to control the resonance of the micro-ring resonators and tune the laser wavelength. On the other hand, the InP gain PIC consists of a semiconductor optical amplifier (SOA) with a highly reflective coating on the left side and an anti-reflective coating on the right side, allowing the emission of light into the Si_3N_4 chip.

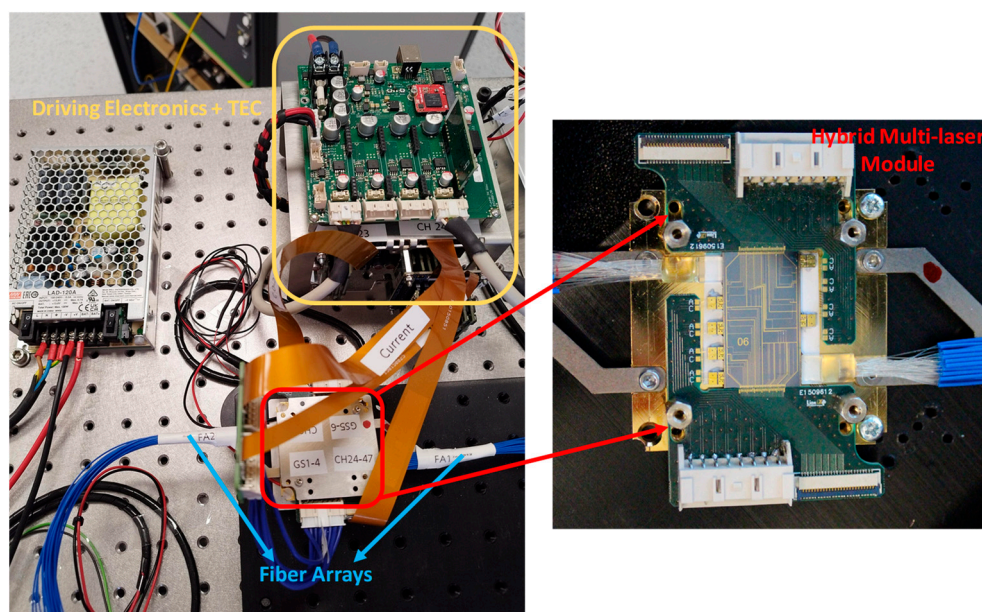


Figure 1. An image of the hybrid multi-laser subsystem, consisting of the laser module and control electronics. On the **right**, a detailed view of the TriPlex[®] photonic integrated circuit is shown, which includes the six InP chips and the Si_3N_4 chip. The image also identifies two fiber arrays: FA1, containing 28 fibers, and FA2, with 24 fibers.

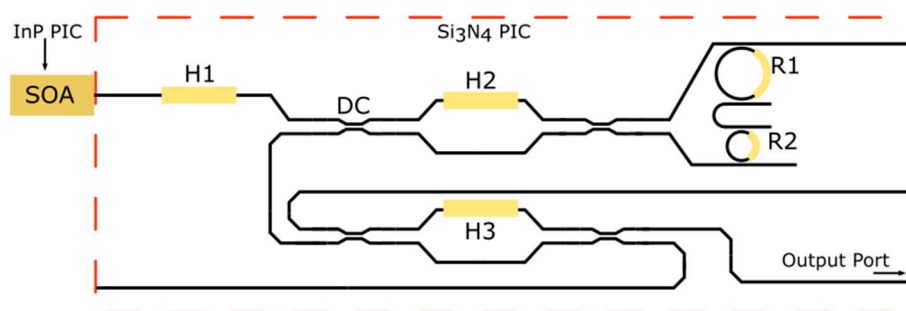


Figure 2. Layout of the InP/ Si_3N_4 hybrid integrated single-gain lasers. The laser cavity is formed by an InP chip (gain section) and a Si_3N_4 chip (dashed red box) as the external cavity. Single-mode operation is achieved using a Vernier filter consisting of two Si_3N_4 micro-ring resonators.

In addition to the four single gain lasers, the PIC includes a dual-gain laser, with its layout shown in Figure 3. As illustrated, the primary difference between the single-gain and dual-gain lasers lies in the addition of a second gain section in the latter. Furthermore, a second thermo-optic actuator, identified as H4, has been incorporated into the Si_3N_4 PIC to control the phase of the light. The actuators utilize the thermo-optic effect, where changes in temperature induce variations in the refractive index of the waveguide material. While the physical length of the waveguide remains unchanged, these refractive index changes

effectively modify the optical path length, allowing precise control over the phase of the propagating light. This capability is critical for fine-tuning the device's performance in applications such as wavelength filtering and resonance alignment. Single-mode operation is also achieved through the Vernier effect, with the FSRs of the two micro-ring resonators matching those of the single-gain lasers.

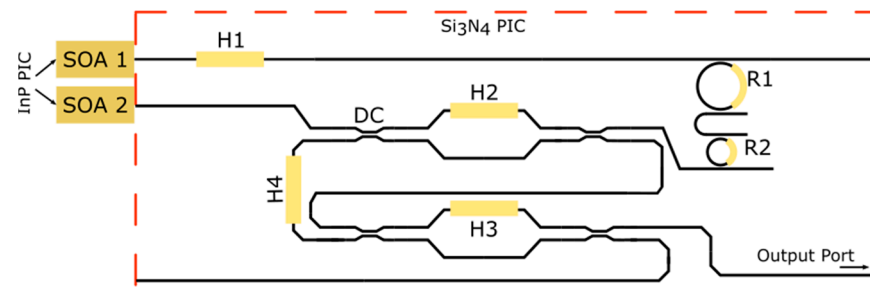


Figure 3. Layout of the InP/Si₃N₄ hybrid integrated dual-gain laser. The laser cavity is formed by two InP chips (gain section) and a Si₃N₄ chip (dashed red box) as the external cavity. Single-mode operation is achieved using a Vernier filter consisting of two Si₃N₄ micro-ring resonators.

3. Experimental Results

This section presents a detailed overview of the experiments performed to evaluate the performance of the hybrid multi-laser module as a local oscillator signal generator. It also includes the results of the characterization of the single-gain lasers used for optical heterodyning, along with a comprehensive description of the experimental setup used in this study. These findings provide a basis for understanding the capabilities and limitations of the system under test.

3.1. Experimental Setup

The experimental setup is depicted in Figure 4. As previously mentioned, three single-gain lasers from the laser module are used for dual LO generation: laser 2 (L2), laser 3 (L3), and laser 4 (L4). The output optical power of each laser is measured using a Thorlabs (New Jersey, United States) PM200 optical power meter (PM). The optical spectrum is observed using a Brillouin Optical Spectrum Analyzer (BOSA) 400 from Aragón Photonics (Zaragoza, Spain), which features an optical resolution of 10 MHz (80 femtometers). This allows for precise observation of the optical spectrum before the signals are directed to an external Finisar (California, United States) XPDV2120RA 50 GHz photodiode for optical-to-electrical (O/E) conversion. After the PD, an electrical spectrum analyzer (ESA), the Rhode & Schwarz (Munich, Germany) FSW-50, with a bandwidth of 50 GHz, is used to record the generated LO signals.

The optical linewidths of the lasers are measured using a delayed self-heterodyne setup, which includes a 40-MHz fiber acousto-optic modulator (AOM) and 6.8 km of single-mode optical fiber between the interferometer arms, as outlined in [17]. This setup allows for precise linewidth measurement by comparing the modulated signal with the reference signal, enabling high-accuracy analysis of the laser performance. However, this coherence length corresponds to a Lorentzian spectrum with a minimum full width at half-maximum (FWHM) linewidth of 14 kHz [22]. As a result, linewidths below this threshold cannot be accurately measured using this setup.

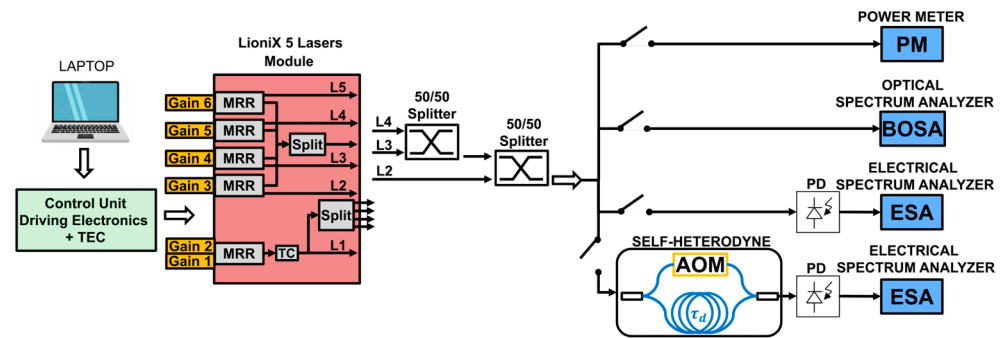


Figure 4. The experimental setup developed for laser characterization and local oscillator (LO) signal generation includes a power meter, used to measure the output power of each laser, as well as optical and electrical spectrum analyzers. The optical spectrum analyzer captures the optical spectrum at the output of the laser module, while the electrical spectrum analyzer records the electrical spectrum after the photodiode. In this work, the single-gain lasers are labeled as L2 (laser 2), L3 (laser 3), and L4 (laser 4).

The TEC and drive electronics are controlled through GUI-based software developed by LioniX. This software facilitates efficient operation and monitoring by linking the electronics control unit to a computer via a USB cable.

3.2. Characterization of Single-Gain Lasers

The characterization of the three lasers used in the optical heterodyne system was performed before the RF signal generation. Figure 5 displays a typical measurement of the fiber-coupled output power of the lasers as a function of the pump current. All three lasers have a threshold current of approximately 11 mA, with maximum output powers of 23 mW for laser 2, 2 mW for laser 3, and 18 mW for laser 4. As shown, even under identical operating conditions, the power levels of each laser differ. These disparities arise from variations in coupling losses between the InP and Si₃N₄ chips for each laser, as well as minor differences in the reflectivity of their respective SOAs. However, by adjusting the current injected into the gain section and fine-tuning the voltages applied to the heaters within each cavity, output powers exceeding 10 dBm can be achieved for each laser, as demonstrated in [17]. The observed power drop in the three curves is attributed to refractive index changes in the InP PIC waveguide, which occur as the current injected into the gain section increases. These refractive index variations induce a slight shift in the emission wavelength, moving it out of resonance with the Vernier filter created by the two ring resonators [20].

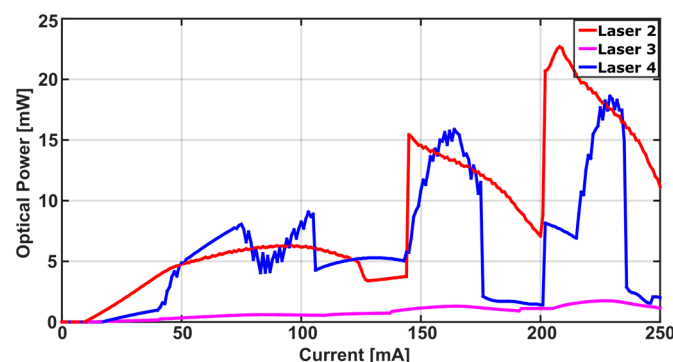


Figure 5. Optical power versus current curve of the three lasers used in the heterodyne system. The lasers exhibit a threshold current of approximately 11 mA, and the power drops indicate mode hops. The measurement was taken at a wavelength of 1550 nm. The curves obtained in this work align with typical behavior observed for these types of lasers.

The V-I characteristic curve was not obtained in this study due to the use of a conventional electronics control module, which lacked the capability to monitor the dynamic resistance of the lasers. However, as outlined in the PDKs provided by the foundries, the average power consumption of the lasers is less than 2 W, with approximately 0.5 W attributed to the gain section and 1.4 W to the actuator heaters. While the current setup does not allow for direct extraction of the V-I curve, this limitation can be addressed by implementing a dedicated interposer PCB equipped with separate power supplies to facilitate such measurements.

For the generation of the LO signals, laser 2 was used as a fixed reference, and the dual RF signals were generated by combining laser 2 with laser 3 and laser 4, respectively. Independent tuning of the generated signals was achieved by adjusting the wavelengths of lasers 3 and 4. Therefore, obtaining the tuning maps for lasers 3 and 4 is essential to determine the frequency tuning ranges of the generated signals. Figure 6 presents the tuning map of the emission wavelength of laser 3. The tuning of this type of laser is achieved by independently varying the voltage applied to the heaters in the micro-ring resonators. To generate the tuning map, the voltage applied to heater R2 was incrementally increased from 0 V to 12 V at each step. Simultaneously, the voltage on heater R1 was varied within the same range, such that for each voltage setting on R1 (ranging from 0 V to 12 V), the voltage on R2 was adjusted from 0 V to 12 V. This approach allowed for independent control over the tuning of both micro-ring resonators, and the voltage on each micro-ring was adjusted in 0.2 V steps. By tuning both micro-rings, a wavelength tuning range of approximately 80 nm was observed in laser 3.

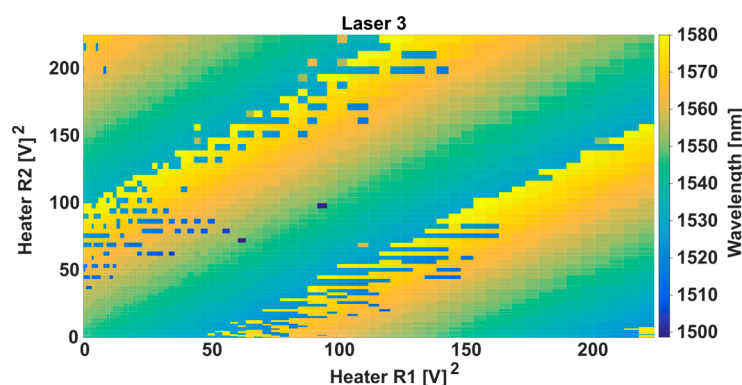


Figure 6. The wavelength tuning map for laser L3 was obtained by varying the voltage applied to the micro-ring resonators in the external cavity. The laser exhibited a tuning range of around 80 nm. During these measurements, the SOA current was held constant at 100 mA.

The tuning map for laser 4 is shown in Figure 7. This laser uses the same tuning mechanism as laser 3. As shown, laser 4 achieves a tuning range of more than 70 nm. As a result, the generated LO signals can cover frequencies from the microwave to the terahertz range.

The electrical linewidth of the generated LO signal in an optical heterodyne system is directly linked to the optical linewidth of each laser employed. To assess the lasers' suitability for LO signal generation, their optical linewidths were measured using the delayed self-heterodyne setup described in the previous subsection. Under free-running conditions, and with only the SOA section of the lasers biased, optical linewidths below 40 kHz were achieved. Figure 8a illustrates the self-heterodyne spectrum for laser 2, centered at 40 MHz. The phase noise of the beat signal was measured using the ESA's built-in phase noise measurement function. The results, presented in Figure 8b, indicate a

phase noise below -60 dBc/Hz at a 100 kHz offset, obtained under the laser's free-running operation regime.

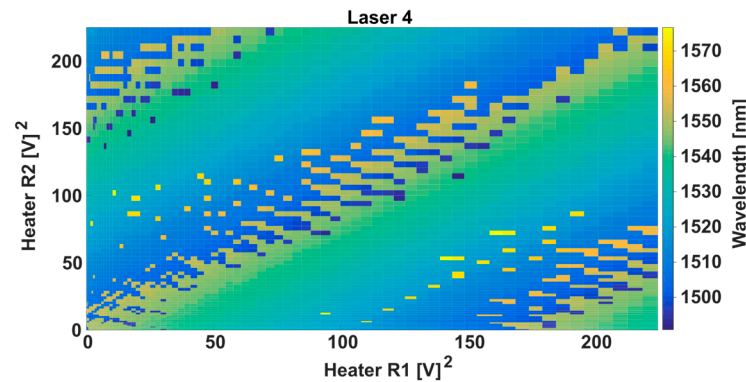


Figure 7. The wavelength tuning map for laser L4 was obtained by varying the voltage applied to the micro-ring resonators in the external cavity. The laser exhibited a tuning range higher than 70 nm. During these measurements, the SOA current was kept constant at 100 mA.

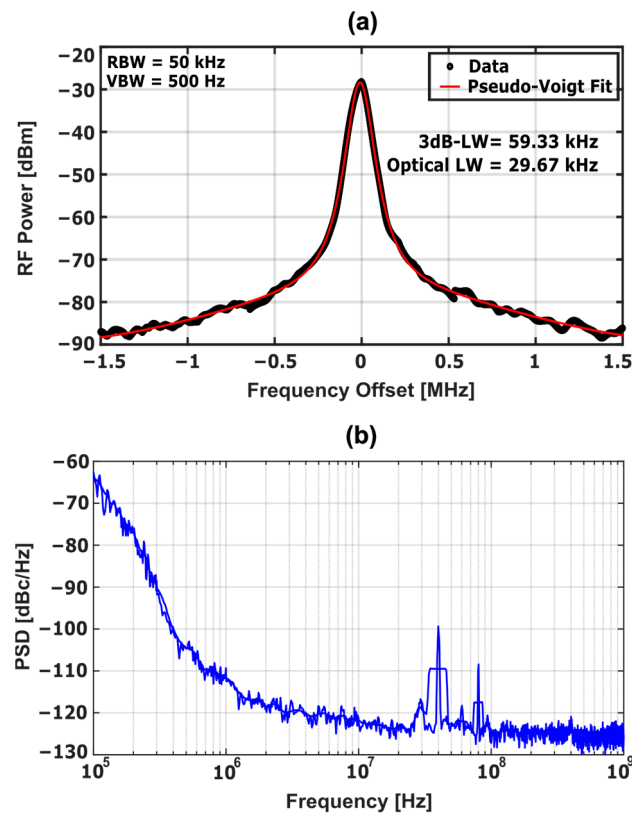


Figure 8. Measurement of the (a) optical linewidth [23] and (b) phase noise of the reference laser used in the optical heterodyne system. Laser 2 exhibits an optical linewidth of 30 kHz, measured using a delayed self-heterodyne setup. Additionally, the phase noise analysis revealed values below -110 dBc/Hz at a 1 MHz offset.

3.3. Dual LO Generation

To experimentally validate the optical heterodyning system, signals were generated at 29 GHz and 41 GHz. These specific frequencies were selected due to their direct relevance to the THORMUX project. Table 1 shows the different operating conditions under which the three lasers were used to generate the signals of interest.

Table 1. Operating conditions of the lasers in the heterodyne system for generating signals at 29 GHz (Ka-band) and 41 GHz (V-band).

Laser	I_{SOA} [mA]	V_{R1} [V]	V_{R2} [V]	V_{H1} [V]	V_{H3} [V]
Laser 2	103	6.6	8	3.6	5.3
Laser 3	152	4.2	13.1	7.21	7
Laser 4	134	12.6	13.6	2.1	10.10

The optical and electrical spectra, measured under these operating conditions, are presented in Figure 9a,b, respectively. In the optical spectrum, each laser exhibits a side-mode suppression ratio (SMSR) exceeding 50 dB, indicating a high degree of spectral purity and stable single-mode operation. This ensures minimal interference from unwanted side modes, which is critical for high-precision applications. Furthermore, as shown in Figure 9b, the two-tone generation at 29 GHz (Ka-band) and 41 GHz (V-band) was successfully achieved. Additionally, a 70 GHz signal is generated due to the beating between laser 3 and laser 4. However, this signal lies outside the bandwidth of the ESA and is therefore not displayed.

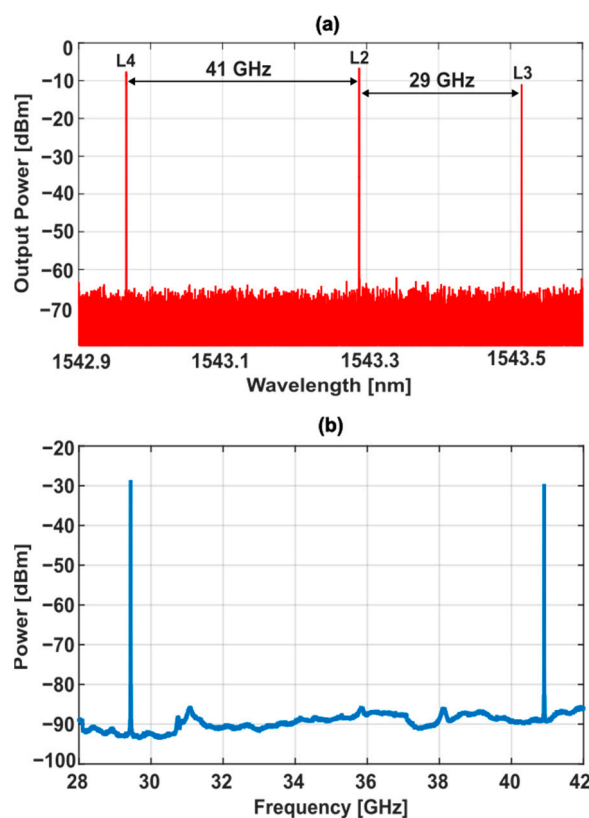


Figure 9. (a) Optical spectrum showing the three optical sources used in the heterodyne system. Laser 2 serves as the reference, while tuning lasers 3 and 4 enables the generation of local oscillator signals in the Ka- and V-bands. (b) Electrical spectrum of the dual local oscillator signals, demonstrating generation of carriers at 29 GHz and 41 GHz [23].

To evaluate the independent tunability of the generated LO signals, the wavelength of laser 3 was gradually increased, thereby increasing its separation from laser 2. This process allowed the Ka-band LO signal to be tuned to three distinct frequencies within the Ka-band: 29 GHz, 31 GHz, and 32 GHz, as shown in Figure 10a. Notably, the tuning of the Ka-band signal did not significantly impact the V-band LO signal, demonstrating the system's capability to maintain stability and independence across multiple frequency bands.

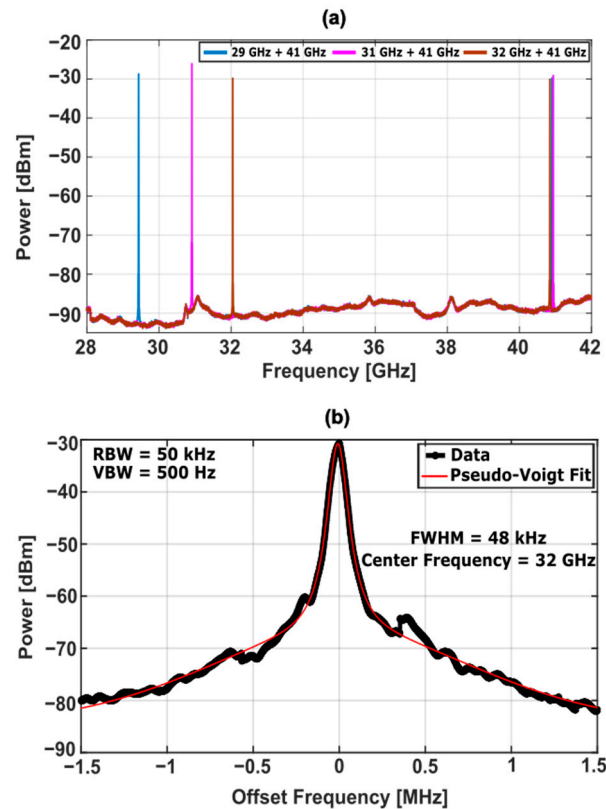


Figure 10. (a) Electrical spectrum demonstrating tunability across the frequency range. By precisely adjusting the emission wavelength of laser 3, the local oscillator signal within the Ka-band was finely tuned from 29 GHz to 31 GHz and 32 GHz. The V-band signal is also displayed. (b) Measurement of the electrical linewidth of the LO signal at 32 GHz.

In addition, the electrical linewidth of the generated signals was measured, showing that all signals have linewidths below 100 kHz. Specifically, the measured linewidths were 45 kHz, 72 kHz, and 48 kHz at 29 GHz, 31 GHz, and 32 GHz, respectively. Figure 10b shows the electrical linewidth measurement for the highest frequency signal generated in the Ka-band. These results underscore the high precision and stability of the generated signals.

Furthermore, since the electrical linewidth reflects the combined optical linewidths of the lasers involved in signal generation, these measurements highlight the potential for significantly reducing optical linewidth through careful optimization of the laser biasing. By precisely adjusting both the gain and heater sections, the optical linewidths can be reduced to less than half of those obtained when only the gain sections are biased. This illustrates that fine-tuning the laser biasing conditions can lead to highly stable, narrow-linewidth signals. In fact, previous studies have observed linewidths in the sub-kHz range with similar hybrid integrated lasers [20]. However, due to limitations in our experimental setup, we were unable to directly measure these ultra-narrow optical linewidths in this work, which explains why the measured linewidth appears broader than the values reported in the literature.

4. Discussion

The hybrid multi-laser module presented in this work demonstrated significant potential for generating multiple high-performance microwave signals, specifically tailored to meet the demands of the THORMUX project. This innovative module integrates advanced optical technologies to achieve precise and reliable signal generation, a crucial requirement for microwave photonics systems.

The InP/Si₃N₄ hybrid integrated lasers exhibit exceptional promise as optical carrier light sources for RF photonics-based multiplexer and demultiplexer systems. Previous studies [17,20] have characterized this type of hybrid integrated lasers, but this work represents, to the best of our knowledge, the first implementation of an integrated hybrid multi-laser module consisting of four single-gain lasers and one dual-gain laser. This module allows multiple RF channels to be handled simultaneously.

The lasers characterized in this work exhibit high output power, with a maximum of 23 mW for laser 2, and an extensive wavelength tuning range spanning the entire C-band. However, this tuning process is not continuous, as mode hops are observed in the wavelength maps. Additionally, the lasers demonstrated narrow optical linewidths of less than 40 kHz in free-running mode. These narrow optical linewidths translate directly into narrow electrical linewidths, below 80 kHz, for local oscillator signals generated through optical heterodyning. This marks a significant improvement over previous optical heterodyne systems that relied on monolithic InP DFB lasers [24,25], showcasing the hybrid module's great performance.

The results obtained for dual local oscillator signal generation further confirm the system's effectiveness at target frequencies, demonstrating its suitability for applications requiring reliable signal generation across multiple frequency bands. The capability to generate high-quality RF signals over diverse frequencies underscores the module's adaptability for various advanced communication and sensing technologies.

An additional advantage of the lasers lies in their ability to exhibit repeatability, a critical factor for practical deployment. Once the initial operating parameters for generating an RF signal at a specific frequency are established, the system can consistently reproduce that frequency whenever those parameters are restored. This reliability holds true even after multiple adjustments to the parameters, ensuring consistent performance over time.

5. Conclusions

This work presented the experimental characterization of three single-gain hybrid integrated lasers for dual local oscillator generation. The optical power versus current curve of the three lasers used in the heterodyne system revealed that the maximum power achieved for laser 3, by only biasing the gain section, was 2 mW. This finding highlights the need for further investigation into the coupling losses between the InP and Si₃N₄ chips of these lasers, as the output power of laser 2 and laser 4 were eleven and nine times higher than this, respectively. Addressing these coupling losses will be a key focus of future studies aimed at enhancing overall system efficiency.

However, through careful control of the current injected into the gain section and precise fine-tuning of the voltages applied to the heaters within the laser cavity, the performance of each laser can be optimized to achieve high output powers and low optical linewidths. These optimizations improved stability, which is a critical factor for the successful implementation of dual local oscillator generation in advanced microwave photonics systems.

It is important to note that while this work presents the wavelength maps for laser 3 and laser 4, all five integrated lasers exhibited a tuning range greater than 70 nm when varying the heater voltages applied to the micro-ring resonators. This extensive tuning range underscores the versatility and adaptability of the system for diverse applications.

In conclusion, this hybrid multi-laser module demonstrates exceptional promise for satellite communication applications, offering enhanced performance, scalability, and reliability. Its ability to generate stable, tunable signals across multiple frequency bands positions it as a transformative technology for next-generation communication networks.

Author Contributions: Conceptualization, C.G.H.R., C.M., I.V., and G.C.; methodology, C.G.H.R., R.B.T., J.C.-C., A.Z., R.C.G., and G.C.; validation, R.B.T., J.C.-C., A.Z., and R.C.G.; writing—original draft preparation, J.C.-C. and A.Z.; writing—review and editing, all the authors; supervision, L.G. and J.M.D.M.; project administration, P.W.L.V.D., C.M., and G.C. All authors have read and agreed to the published version of the manuscript.

Funding: This work has been supported by the European Space Agency through the TRP program “Tuneable Photonic RF Demultiplexer for Broadband Satellites—THORMUX” (GA 870421), by the European Union through the projects TERA6G (GA 101096949), SPRINTER (GA 101070581), and POLYNICES (G.A. 101070549), and by a Spanish national project, “6G-Xtreme” (Ref. TSI-063000-2021-136).

Institutional Review Board Statement: Not applicable.

Informed Consent Statement: Not applicable.

Data Availability Statement: No new data were created during the construction of the manuscript.

Acknowledgments: We thank Maaïke Benedictus for her help with the control software.

Conflicts of Interest: Authors Charoula Mitsolidou, Ilka Visscher, Roelof B. Timens, Paulus W. L. Van Dijk, and Chris G. H. Roeloffzen were employed by the company Lionix International B.V. The remaining authors declare that the research was conducted in the absence of any commercial or financial relationships that could be construed as a potential conflict of interest.

References

1. Anzalchi, J.; Inigo, P.; Roy, B. Application of photonics in next generation telecommunication satellites payloads. *Int. Conf. Space Opt. (ICSO)* **2014**, *10563*, 1063–1071.
2. Vono, S.; Di Paolo, G.; Piccinni, M.; Pisano, A.; Sotom, M.; Aveline, M.; Ginestet, P. Towards telecommunication payloads with photonic technologies. *Int. Conf. Space Opt. (ICSO)* **2014**, *10563*, 1054–1062.
3. Logan Jr, R.T.; Basuita, D. Mass-reduction of high-speed spacecraft datalinks enabled by rugged photonic transceivers. *Int. Conf. Space Opt. (ICSO)* **2018**, *11180*, 1618–1628.
4. Marpaung, D.; Yao, J.; Capmany, J. Integrated microwave photonics. *Nat. Photonics* **2019**, *13*, 80–90. [[CrossRef](#)]
5. Zhu, D.; Shao, L.; Yu, M.; Cheng, R.; Desiatov, B.; Xin, C.J.; Hu, Y.; Holzgrafe, J.; Ghosh, S.; Shams-Ansari, A.; et al. Integrated photonics on thin-film lithium niobate. *Adv. Opt. Photonics* **2021**, *13*, 242–352. [[CrossRef](#)]
6. Vazimali, M.G.; Fathpour, S. Applications of thin-film lithium niobate in nonlinear integrated photonics. *Adv. Photonics* **2022**, *4*, 034001. [[CrossRef](#)]
7. Augustin, L.M.; Santos, R.; Den Haan, E.; Kleijn, S.; Thijs, P.J.; Latkowski, S.; Zhao, D.; Yao, W.; Bolk, J.; Ambrosius, H.; et al. InP-based generic foundry platform for photonic integrated circuits. *IEEE J. Sel. Top. Quantum Electron.* **2017**, *24*, 1–10. [[CrossRef](#)]
8. Smit, M.; Williams, K.; Van Der Tol, J. Past, present, and future of InP-based photonic integration. *APL Photonics* **2019**, 1–10. [[CrossRef](#)]
9. Sharma, T.; Wang, J.; Kaushik, B.K.; Cheng, Z.; Kumar, R.; Wei, Z.; Li, X. Review of recent progress on silicon nitride-based photonic integrated circuits. *IEEE Access* **2020**, *8*, 195436–195446. [[CrossRef](#)]
10. Xiang, C.; Jin, W.; Bowers, J.E. Silicon nitride passive and active photonic integrated circuits: Trends and prospects. *Photonics Res.* **2022**, *10*, A82–A96. [[CrossRef](#)]
11. Zhu, Y.; Zhao, Y.; Zhu, L. Loss induced coherent combining in InP-Si₃N₄ hybrid platform. *Sci. Rep.* **2018**, *8*, 878. [[CrossRef](#)]
12. Ibrahimi, Y.; Boust, S.; Wilmart, Q.; Paret, J.F.; Garreau, A.; Mekhazni, K.; Fortin, C.; Duport, F.; Fedeli, J.-M.; Sciancalepore, C.; et al. Low FSR mode-locked laser based on InP-Si₃N₄ hybrid integration. *J. Light. Technol.* **2021**, *39*, 7573–7580. [[CrossRef](#)]
13. Göbel, T.; Stanze, D.; Troppenz, U.; Kreissl, J.; Sartorius, B.; Schell, M. Integrated continuous-wave THz control unit with 1 THz tuning range. In Proceedings of the 2012 37th International Conference on Infrared, Millimeter, and Terahertz Waves, Wollongong, NSW, Australia, 23–28 September 2012; pp. 1–3.
14. Theurer, M.; Göbel, T.; Stanze, D.; Troppenz, U.; Soares, F.; Grote, N.; Schell, M. Photonic-integrated circuit for continuous-wave THz generation. *Opt. Lett.* **2013**, *38*, 3724–3726. [[CrossRef](#)]
15. Nagatsuma, T.; Ducournau, G.; Renaud, C.C. Advances in terahertz communications accelerated by photonics. *Nat. Photonics* **2016**, *10*, 371–379. [[CrossRef](#)]
16. Delmade, A.; Browning, C.; Verole, T.; Poette, J.; Farhang, A.; Elwan, H.H.; Koilpillai, R.D.; Aubin, G.; Lelarge, F.; Ramdane, A.; et al. Optical heterodyne analog radio-over-fiber link for millimeter-wave wireless systems. *J. Light. Technol.* **2020**, *39*, 465–474. [[CrossRef](#)]

17. Guzmán, R.; González, L.; Zarzuelo, A.; Cesar Cuello, J.; Ali, M.; Visscher, I.; Grootjans, R.; Epping, J.P.; Roeloffzen, C.G.H.; Carpintero, G. Widely tunable RF signal generation using an InP/Si₃N₄ hybrid integrated dual-wavelength optical heterodyne source. *J. Light. Technol.* **2021**, *39*, 7664–7671. [[CrossRef](#)]
18. Lipka, M.; Parniak, M.; Wasilewski, W. Optical frequency locked loop for long-term stabilization of broad-line DFB laser frequency difference. *Appl. Phys. B* **2017**, *123*, 1–7. [[CrossRef](#)]
19. Wörhoff, K.; Heideman, R.G.; Leinse, A.; Hoekman, M. TriPleX: A versatile dielectric photonic platform. *Adv. Opt. Technol.* **2015**, *4*, 189–207. [[CrossRef](#)]
20. Fan, Y.; van Rees, A.; Van der Slot, P.J.M.; Mak, J.; Oldenbeuving, R.M.; Hoekman, M.; Geskus, D.; Roeloffzen, C.G.; Boller, K.J. Hybrid integrated InP-Si₃N₄ diode laser with a 40-Hz intrinsic linewidth. *Opt. Express* **2020**, *28*, 21713–21728. [[CrossRef](#)] [[PubMed](#)]
21. Gomes, A.D.; Bartelt, H.; Frazão, O. Optical Vernier effect: Recent advances and developments. *Laser Photonics Rev.* **2021**, *15*, 2000588. [[CrossRef](#)]
22. Saleh, B.E.; Teich, M.C. *Fundamentals of Photonics*; John Wiley & Sons: Hoboken, NJ, USA, 2019.
23. César-Cuello, J.; Zarzuelo, A.; Mitsolidou, C.; Guerrero, L.G.; Timens, R.B.; Van Dijk, P.W.; Roeloffzen, C.G.; Delgado, J.M.; Carpintero, G. Integrated Photonics-Based Electrical Multicarrier Generation System for Satellite Communications in the Ka and V Bands. In Proceedings of the International Topical Meeting on Microwave Photonics (MWP), Pisa, Italy, 17–20 September 2024; pp. 1–4.
24. Van Dijk, F.; Accard, A.; Enard, A.; Drisse, O.; Make, D.; Lelarge, F. Monolithic dual wavelength DFB lasers for narrow linewidth heterodyne beat-note generation. In Proceedings of the International Topical Meeting on Microwave Photonics, Singapore, 18–21 October 2011; pp. 73–76.
25. Lo, Y.H.; Wu, Y.C.; Hsu, S.C.; Hwang, Y.C.; Chen, B.C.; Lin, C.C. Tunable microwave generation of a monolithic dual-wavelength distributed feedback laser. *Opt. Express* **2014**, *22*, 13125–13137. [[CrossRef](#)]

Disclaimer/Publisher’s Note: The statements, opinions and data contained in all publications are solely those of the individual author(s) and contributor(s) and not of MDPI and/or the editor(s). MDPI and/or the editor(s) disclaim responsibility for any injury to people or property resulting from any ideas, methods, instructions or products referred to in the content.